Polymer Bulletin (2020) 77:901–917
https://doi.org/10.1007/s00289-019-02778-z

ORIGINAL PAPER

Effect of filler type on properties of PBAT/organoclay nanocomposites

Tiago T. Santos[1] · Tatiara G. Almeida[1] · Dayanne D. S. Morais[1] · Fernão D. Magalhães[2] · Rui M. Guedes[2] · Eduardo L. Canedo[3] · Laura H. Carvalho[3]

Received: 12 November 2018 / Revised: 1 April 2019 / Accepted: 8 April 2019 / Published online: 13 April 2019

Abstract

The goal of this study is to evaluate the effect of different organoclays on the properties of poly(butylene adipate-*co*-terephthalate) (PBAT)/organoclay systems. PBAT/organoclay nanocomposites containing 2.5, 5.0 and 7.5% of three different commercial organically modified clays (Cloisite® C10A, C20A and C30B) were prepared as a masterbatch in a laboratory internal mixer, let down to the appropriate concentration in a co-rotating twin-screw extruder, and test specimens were injection molded. Nanocomposites were characterized by X-ray diffraction (XRD), transmission electron microscopy (TEM), differential scanning calorimetry (DSC), thermogravimetry (TGA) and dynamic mechanical analysis (DMA) as a function of clay identity and content. XRD results showed a significant increase in the interlayer spacing of the clay, suggesting that intercalated structures were obtained with all systems investigated, as confirmed by TEM. Organoclay incorporation into PBAT resulted in lower melt crystallization temperatures compared with the neat polymer, particularly in PBAT/C30B nanocomposites, slightly improved thermal stability, increased stiffness and no changes in the glass transition temperature. Compounding PBAT with up to 7.5% of C10A, C20A or C30B organoclays is an option to improve the performance of PBAT.

Keywords PBAT · Organoclay · Nanocomposites · Intercalation

Electronic supplementary material The online version of this article (https://doi.org/10.1007/s00289-019-02778-z) contains supplementary material, which is available to authorized users.

✉ Tatiara G. Almeida
tatiaraalmeida@gmail.com

[1] Graduate Program in Materials Science and Engineering, Federal University of Campina Grande, Campina Grande, PB 58429-140, Brazil

[2] Faculty of Engineering, University of Porto, 4200-465 Porto, Portugal

[3] Department of Materials Engineering, Federal University of Campina Grande, Campina Grande, PB 58429-140, Brazil

Introduction

Global warming awareness, environmental and waste issues management and the decline of fossil resources are some of the reasons for the increasing use of biodegradable polymers on making sustainable products. The main advantages of using these polymers are their biodegradability, i.e., their susceptibility to attacks by fungus and microorganisms when disposed in adequate environment [1] and their mechanical and thermal properties, which are comparable to many petroleum-based plastics. Biodegradable polymers have great commercial potential and may soon be competing with commodity plastics. Despite several advantages, some of the properties of these plastics such as brittleness, low heat distortion temperature, high gas permeability, low melt viscosity, among others, restrict their use in a wide-range of applications [2, 3].

Poly(butylene adipate-co-terephthalate) (PBAT) is an aliphatic-aromatic biodegradable copolyester based on terephthalic acid, adipic acid and 1,4-butanediol molecular units. PBAT is flexible and has a higher elongation at break than most biodegradable polyesters, such as poly(lactic acid) (PLA) and polybutylene succinate (PBS), being suitable for food packaging and agricultural films. The main limitations of this polymer toward these applications are its high water vapor permeability and its relatively low rate of biodegradation compared with some other biodegradable materials. We have recently shown that PBAT biodegradability in soil is significantly improved if the polymer is exposed to UV radiation prior to its burial [4]. PBAT/organoclay systems are considered to be sustainable as this matrix is biodegradable and the layered clay is a naturally abundant material whose degradation products are not harmful to soil. Polymer nanocomposites are among the routes to improve some of the properties of conventional and biodegradable polymers. Organoclay addition to PBAT may overcome the drawbacks of neat PBAT, improving several of its properties and thus enlarging its application fields [5–10]. In this work, three different organoclays were added to PBAT, and the properties of the nanocomposites obtained were determined. PBAT was chosen as the matrix because of its mechanical and biodegradation characteristics which can be improved by the organoclay incorporation.

Nanocomposites exhibit special mechanical, thermal, optical, physical and chemical properties, allowing the extensive use of these materials in automotive, packaging and building industries [6–8, 11]. Montmorillonites are among the most common nanofillers used in the preparation of polymer nanocomposites. These clays are layered silicate structures whose interlayer cations can be exchanged by cationic surfactants such as alkylammonium salts. As a result of the cationic exchange of natural montmorillonites with organic salts, organoclays with increased interlayer spacings and improved compatibility with polymers are obtained, leading to an easier intercalation of the polymer chains between the clay mineral layers [12, 13], expanding its basal distance and facilitating intercalation and/or exfoliation. The organoclays chosen to perform this work (Cloisite 10A, 20A and 30B) are commercial organically modified montmorillonites widely used in polymer nanocomposites [6–12, 14]. They are based on a sodium

montmorillonite modified with different alkyl ammonium salts as described in the experimental section.

Several studies are reported on the preparation of PBAT/organoclay nanocomposites. Most of these studies aim to optimize the properties of these systems with the addition of small load content (1–10%) [6, 7, 15–18]. However, significant improvements in the properties of nanocomposites are only achieved when a high level of interaction of the polymer chains within the lamellae of the silicates is achieved, and these improvements are dependent both on the state of dispersion of the organoclays in the polymer matrix and on the nature and composition of the organoclay used.

The goal of this contribution is to investigate the effect of three different types of organoclays on the physical, rheological, thermal, crystalline properties and morphology of PBAT/organoclay composites.

Experimental

Materials

The polymeric matrix employed was poly(butylene adipate-*co*-terephthalate) (PBAT), supplied by BASF (Ludwigshafen, Germany) as Ecoflex® F Blend 1200. According to the manufacturer, this copolyester has a density of 1.26 g/cm^3, melting point below 140 °C and melt flow rate between 2.7 to 4.9 dg/min (ASTM D1238, 190 °C/2.16 kg) [5].

Three different organically modified montmorillonites (OC) supplied as fine whitish powders (90% mass with particle size ≤ 13 µm) and less than 2% moisture content by BYL Southern Clay Products (Gonzalez TX, USA) were used to prepare the nanocomposites. The difference between them is the quaternary ammonium cation used to substitute the inorganic cation in the interlayer gap [14].

- Cloisite 10A (C10A): dimethyl benzyl alkyl ammonium cation
- Cloisite 20A (C20A): dimethyl dialkyl ammonium cation
- Cloisite 30B (C30B): methyl bis-2-hydroxyethyl alkyl ammonium cation

Figure 1 shows the chemical structures of organoclays where T is tallow, and it is a mixture of C_{18}, C_{16} and C_{14} homologs. HT is hydrogenated tallow.

Some properties of these organoclays are listed in Table 1 [19].

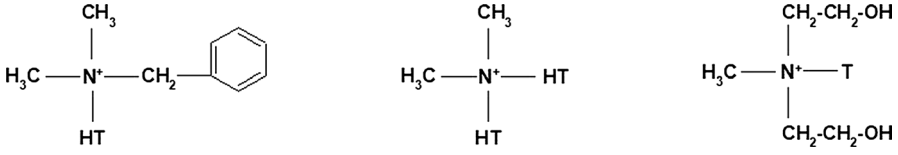

Fig. 1 Chemical structures of organoclays: C10A (left), C20A (center) and C30B (right)

Table 1 Organoclays properties

Property	Unit	C10A	C20A	C30B
Density	(g/cm^3)	1.90	1.77	1.98
Apparent density	(g/cm^3)	0.16	0.12	0.23
Cation exchange capacity	(meq/g)	1.25	0.95	0.90

Sample preparation

Masterbatches containing 50% w/w organoclay content (C10A, C20A or C30B) were prepared in a Haake Rheomix 3000 laboratory internal mixer fitted with high intensity "roller" rotors, operating at a nominal speed of 120 rpm for 15 min, with the mixing chamber wall kept at 170 °C and a fill factor of 70% estimated at feed conditions. Each masterbatch was ground and let down to 2.5, 5.0 and 7.5% w/w organoclay content in a 22 mm, 38 L/D co-rotating NZ twin-screw extruder, model SJ-20, operated at 480 rpm, flow rate of 10.0 kg/h with the barrel temperature maintained at 160 °C. Literature reports that nanocomposites are obtained at low loading levels (<10% w/w), preferable ≤ 5%, as aggregation and lower properties tend to occur at high loadings [7]. The stepwise processing used to obtain the nanocomposites in this work, i.e., preparation of masterbatches and dilution, was intentionally defined in order to promote a greater dispersion of the clays in the polymer matrix, with intense processing in both the internal mixer and the extruder. The materials processed in the extruder were injection molded in an Arburg Allrounder 270 V equipment operated at 140/160/160/165/170 °C in its heating zones, with cooling time of 50 s and mold temperature of 30 °C. Type I tensile test specimens according to ASTM D638 standard were obtained.

Characterization methods

X-Ray Diffraction (XRD)

The basal spacing of the organoclays and nanocomposites were determined with a Shimadzu XRD-6000 X-ray diffraction equipment. The source of the incident radiation was CuKα with a wavelength of 0.154 nm. Data were acquired in an angular range (2θ) between 2° and 12° under scan rate of 2°/min, and d_{001} was computed from Bragg's law.

Transmission electron microscopy (TEM)

Transmission electron microscopy was performed on a FEI Morgani 268D apparatus, operating at an accelerating voltage of 100 kV. TEM samples were taken from the center of the tensile test specimen as trapezoidal shape trimmings.

Differential scanning calorimetry (DSC)

DSC tests were performed in a TA Instruments DSC Q20 equipment operating under nitrogen flux (50 mL/min), on samples of approximately 5 mg. A three-stage nonisothermal program was used: heating from 25 to 200 °C, cooling to 25 °C and reheating to 200 °C, with heating/cooling rate of 8 °C/min. Parameters for crystallization (C1) and melting (F2) of PBAT in PBAT/organoclay compounds were determined using a custom software. The detailed methodology is reported in Canedo et al. [20] and was widely tested [21–25]. The latent heat of melting used for the hypothetically 100% crystalline PBAT was 114 J/g [26].

Thermogravimetry (TG)

Thermogravimetric experiments were conducted on Shimadzu TGA S1H apparatus operating from 30 to 700 °C for organoclays and from 30 to 600 °C for neat PBAT and PBAT/organoclay systems. All experiments were performed with $\emptyset = 10$ °C/min heating rate in nitrogen atmosphere (100 mL/min) using α-alumina crucibles.

Stages of mass loss were identified and masses m_1* and m_2* and T_1 and T_2 temperatures at the beginning and end of each stage determined by extrapolating the tangent to the curve m*(T). The mass loss Δm and the mean temperature $T_{½}$ are then estimated for each stage, as shown by Eqs. 1 and 2:

$$\Delta m = m_1^* - m_2^* \tag{1}$$

$$T_{1/2} = {}^1\!/_2\left(T_1 + T_2\right) \tag{2}$$

In addition, the mass loss rate R (mg min^{-1}) was evaluated, Eq. 3:

$$R = \frac{\emptyset \Delta m}{T_2 - T_1} \tag{3}$$

Dynamic mechanical analysis

Dynamical mechanical measurements, performed in three-point bending mode, were performed in 40 × 9.8 × 3.25 mm (length × thickness × width) rectangular test specimens using an Artemis (Netsch) DMA 242 E equipment in the temperature range of − 80 to 90 °C with a heating rate of 2 °C/min under a controlled atmosphere of nitrogen, in the frequency of 1 Hz.

Results and discussion

X-Ray Diffraction (XRD)

Diffraction peaks of the organoclays and nanocomposites are shown in Fig. 2. Numerical values of basal distance (d_{001}) for the first diffraction peak were determined and are reported in Table 2.

A significant displacement of the diffraction peak to smaller angles (higher basal spacing) was observed for all nanocomposites investigated. Increases in basal interplanar distance up to 100%, 38% and 80% in systems containing C10A, C20A and C30B clays were obtained. Irrespective of organoclay identity, very similar clay basal distances were obtained in all compounds: 3.6 ± 0.1, suggesting

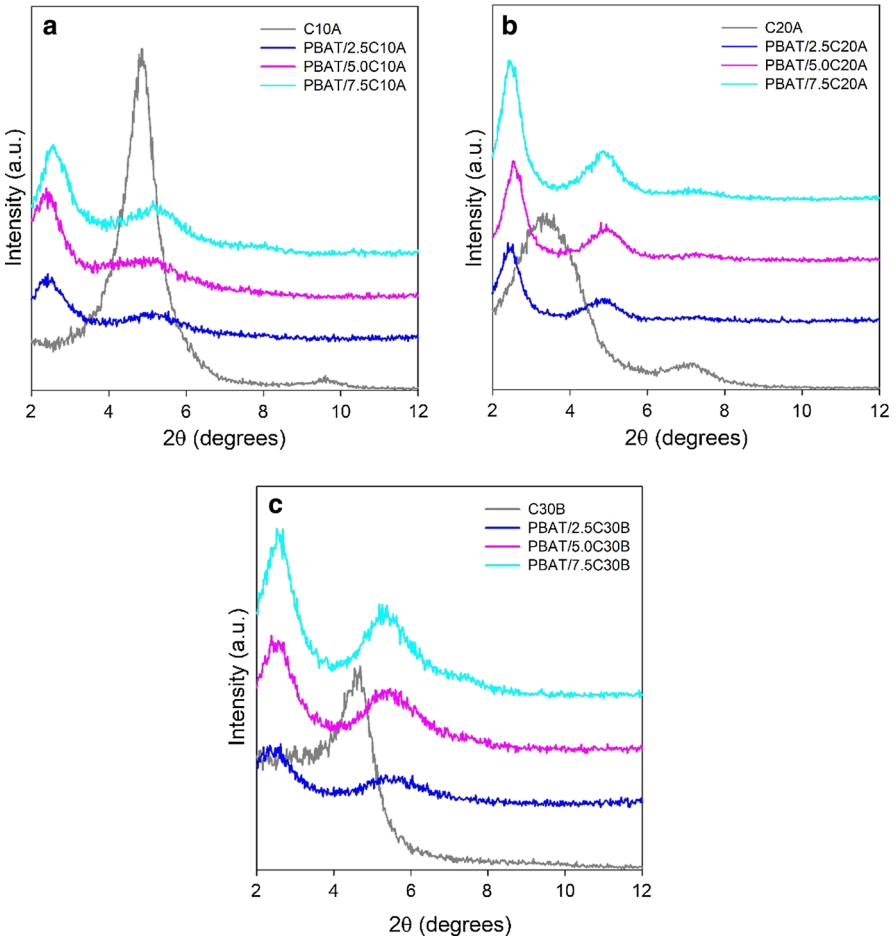

Fig. 2 Diffraction peaks of the organoclays and nanocomposites with C10A (**a**), C20A (**b**) and C30B (**c**)

Table 2 Basal distance (d_{001}) of organoclays and nanocomposites

System	C10A	C20A	C30B
OC	1.82	2.65	1.92
PBAT/2.5% OC	3.68	3.57	3.71
PBAT/5.0% OC	3.79	3.43	3.53
PBAT/7.5% OC	3.41	3.66	3.47

similar and significant degree of intercalation with negligible exfoliation as d_{001} peaks were observed for all nanocomposites investigated [8, 27–29].

Transmission electron microscopy (TEM)

Figure 3a–f shows TEM images of PBAT/organoclay nanocomposites and allows a direct visual observation of the dispersion of the organoclays in the PBAT matrix.

The nanocomposites exhibit a multilayer morphology composed of alternating polymer and inorganic layers (indicated by arrows) and some dispersed layers, revealing a significant level of intercalation and partial exfoliation of these organoclays with PBAT. The increase in organoclay content in the nanocomposites slightly improves the level of dispersion, particularly for the PBAT/C30B system and is probably associated with the slightly more polar nature of this particular organoclay [7, 13, 16]. These results are consistent with XRD results.

Thermal characterization

Figure 4 shows the plot of heat flow versus time during the cooling and reheating temperature stages for PBAT and its nanocomposites.

Single crystallization melting peaks (coded C1) during the cooling stage and melting peaks on reheating (coded F2) were observed in all studied samples. Shallow melting peaks were obtained, indicating a low-crystallinity system. This was expected as PBAT is a random copolymer. Crystallization and melting peaks during reheating were analyzed in detail to determine several transition parameters.

Crystallization event

Numerical results for the crystallization peak from for neat PBAT and the nanocomposites investigated are displayed in Table S1 (Supplementary Information). Relative crystallinity and crystallization rates as a function of temperature for the crystallization event of PBAT and its nanocomposites are shown in Fig. 5.

Figure 6 illustrates two characteristic parameters of the crystallization event for all samples studied: the peak crystallization temperature and the degree of crystallinity.

The data indicates that, compared to neat PBAT, crystallization temperature increases upon compounding for all systems investigated and tended to increase with filler content, particularly for the PBAT/C30B system. In general, *T*c

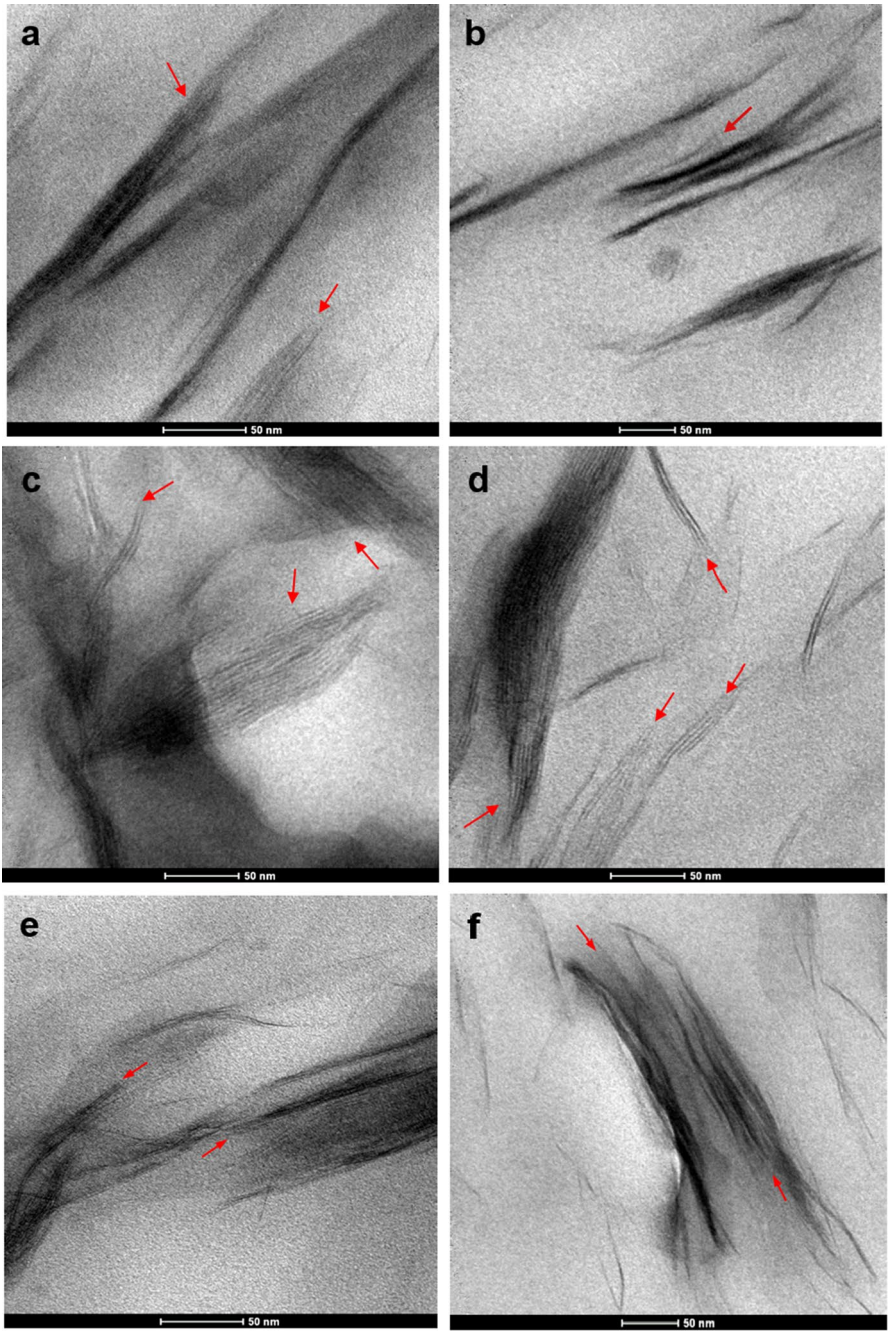

Fig. 3 TEM micrographs for nanocomposites: PBAT/2.5C10A (**a**), PBAT/7.5C10A (**b**), PBAT/2.5C20A (**c**), PBAT/7.5C20A (**d**), PBAT/2.5C30B (**e**) and PBAT/7.5C30B (**f**)

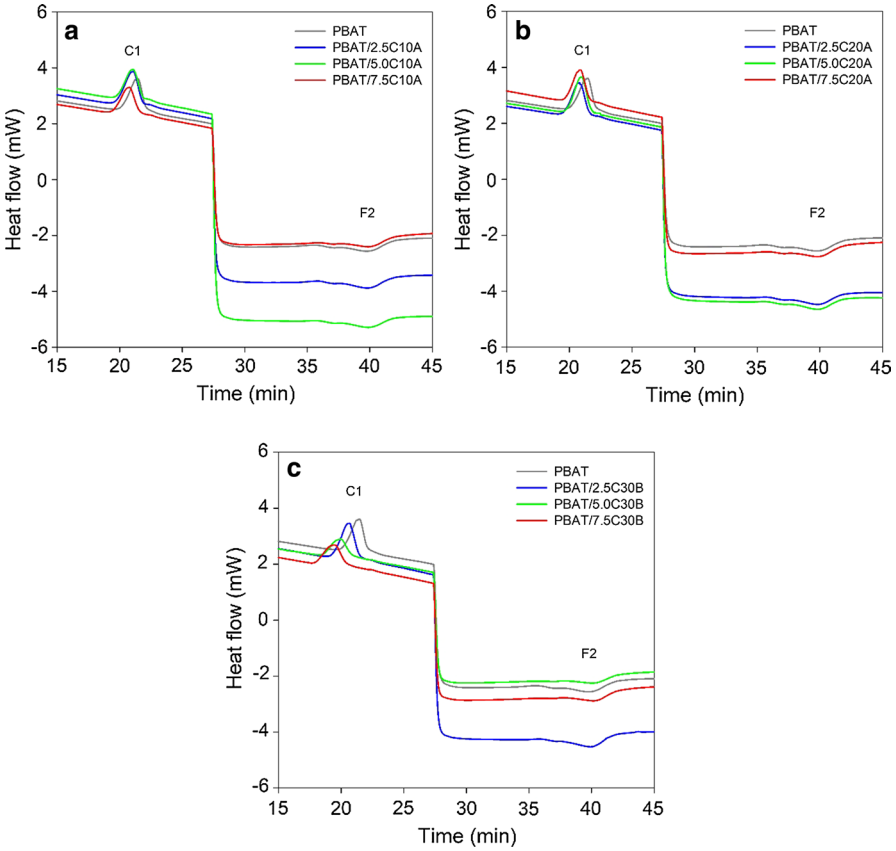

Fig. 4 Heat flow versus time for PBAT and nanocomposites C10A (**a**), C20A (**b**) and C30B (**c**) (exothermic peaks up)

increased in the following order: PBAT/C30B>PBAT/C20A≥PBAT/C10A. *Tc* increased by approximately 4 to 5 °C for composites with C10A and C20A and by 6.5 to 15.8 °C for C30B nanocomposites, depending on clay level. This suggests a stronger nucleating effect of this particular solid particulate load, which may be associated with the more hydrophilic nature of C30B compared with C10A and C20A [30].

Changes in degree of crystallinity are small, ambiguous and within the detection accuracy of the equipment. Degree of crystallinity increases from 2 to 3% for the C10A and C20A compounds and a decrease of 1.4% for the C30B compounds were observed. In general, the degree of crystallinity of the nanocomposites was higher than that of the neat matrix. The addition of nucleating fillers did not significantly increase the degree of crystallinity of PBAT as expected as this is a low-crystallinity random copolymer and as such has an inherently irregular in structure which prevents high crystallinity.

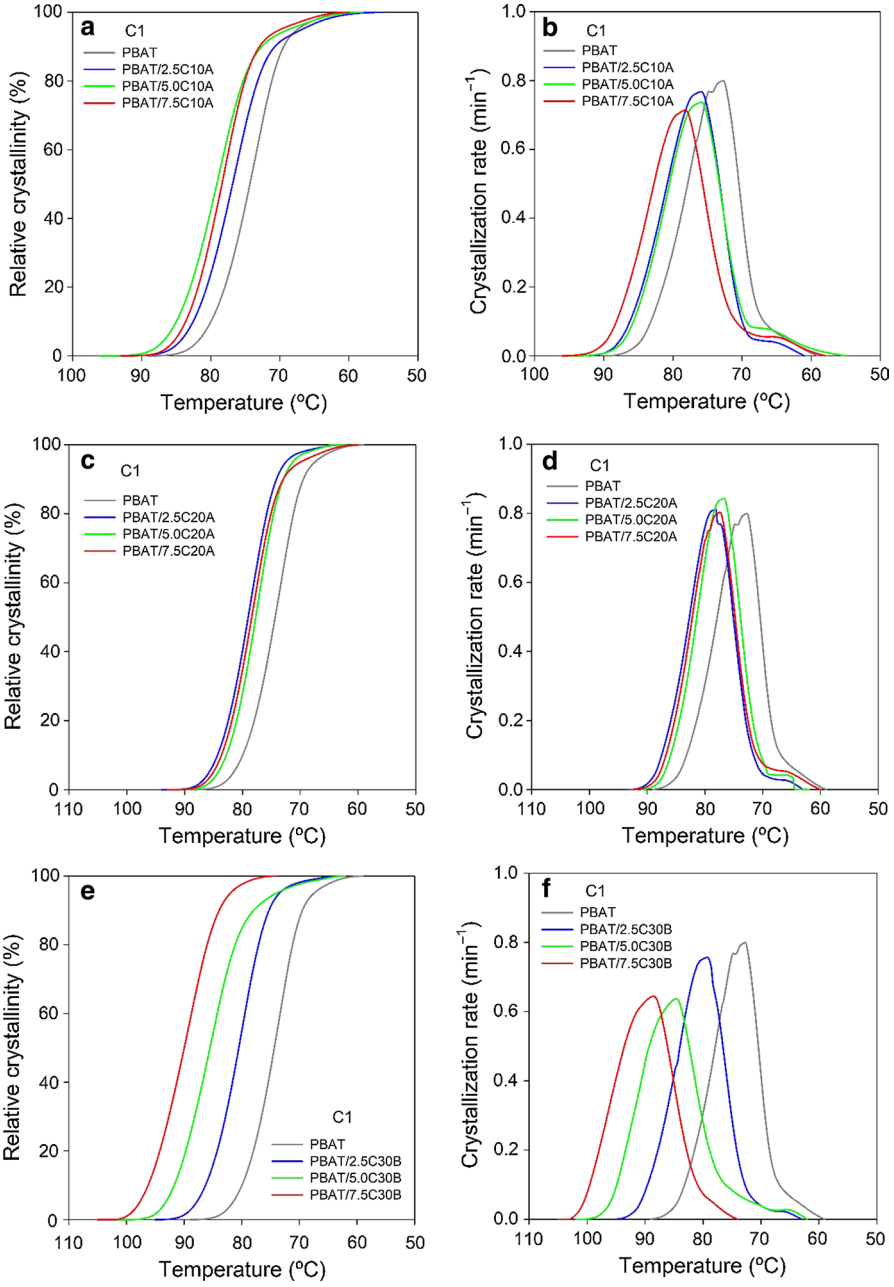

Fig. 5 Relative crystallinity and crystallization rate versus temperature on cooling for PBAT and PBAT/organoclay nanocomposites with C10A (**a**, **b**), C20A (**c**, **d**) and C30B (**e**, **f**)

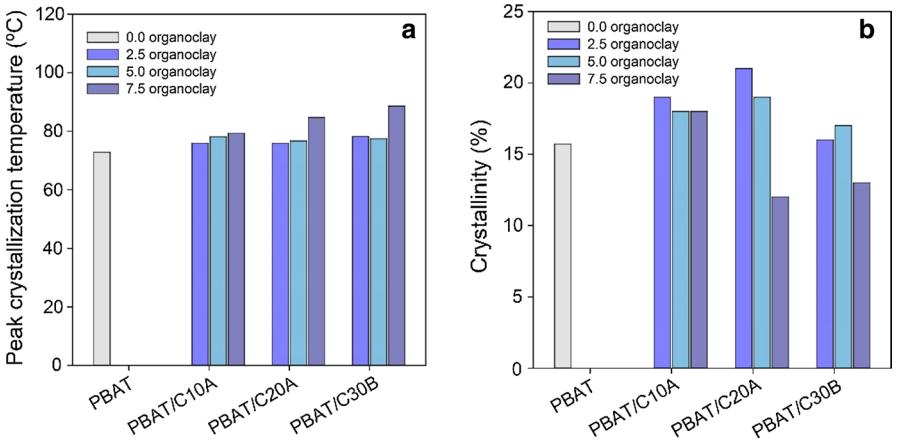

Fig. 6 Peak crystallization temperature (**a**) and crystallinity (**b**) for PBAT and nanocomposites

Melting event

Numerical results for the melting peak of PBAT and of the nanocomposites investigated are reported in Table S2 (Supplementary Information). The same study used for the cooling event was performed for the second melting (F2) event, as shown in Fig. 7.

Peak melting temperature and degree of crystallinity obtained in the second melting for all tested samples are shown in Fig. 8.

Our data indicates that melting was hardly affected by clay incorporation and takes place between 85 and 145 °C for all samples. Melting temperature was shown to be independent of organoclay identity and content. Similar to what was observed for the crystallization event, in general, very slight increases in degree of crystallinity during the second melting were observed for the nanocomposites. These changes were not significant and are associated with the chemical structure of PBAT (a random copolymer) preventing high degrees of crystallinity.

Thermogravimetry

TG curves of the neat PBAT and nanocomposites are shown in Fig. 9.

Table S3 (Supplementary Information) displays the initial, maximum and mean decomposition temperatures values, mass loss and residue at 600 °C. The mass loss observed in the TG curve of PBAT occurs in a single stage at a mean temperature of 390 °C, losing more than 80% of its mass between 370 and 420 °C at a relatively high rate of mass loss of about 16%/min. The thermal stability of PBAT slightly improved upon organoclay incorporation; mean increases in $T_{½}$ of 9 °C, 5 °C and 2 °C were observed for the composites with C10A, C20A and C30B and appeared to be independent of clay concentration. It is believed that the dispersed clay generates a barrier which delays the release of thermal degradation products in comparison with the pristine polymer [31, 32].

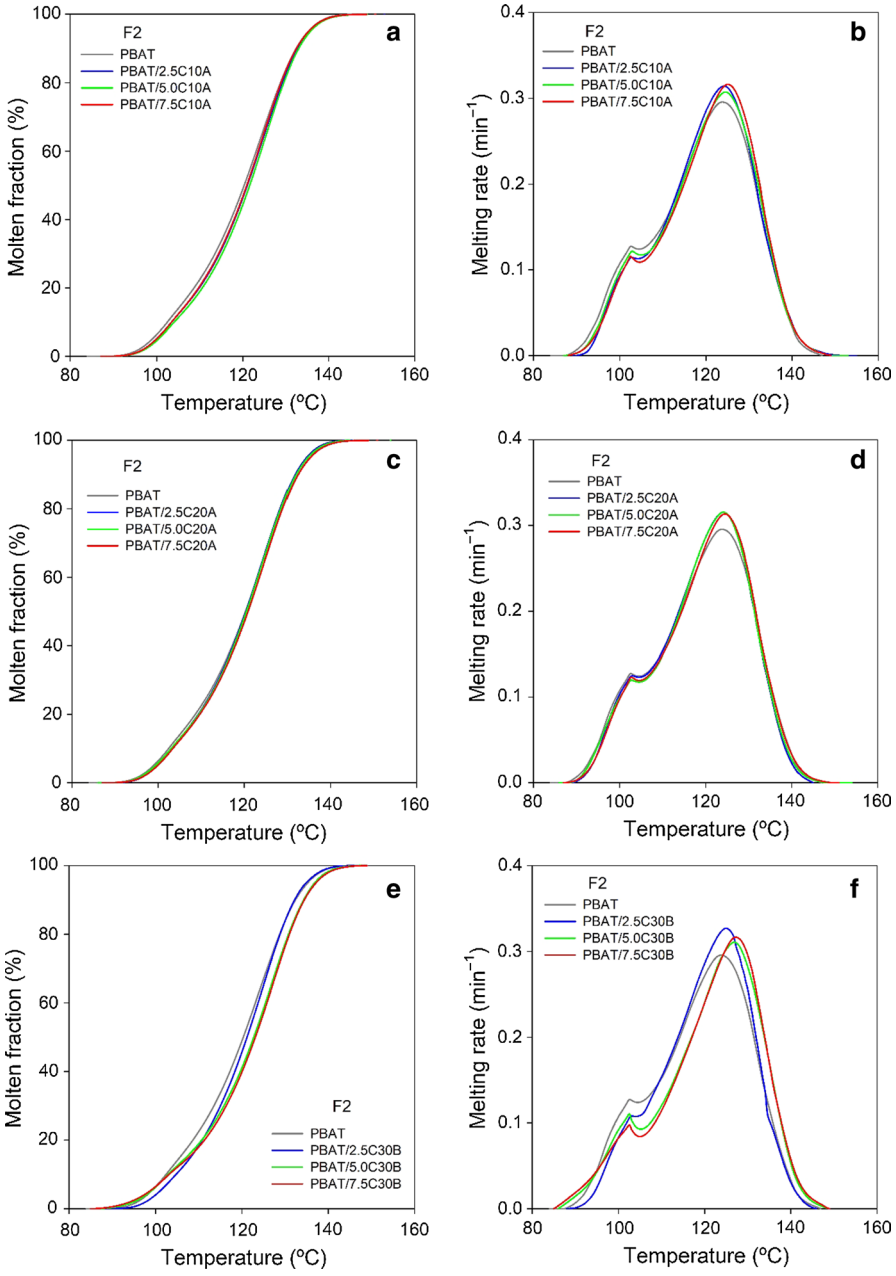

Fig. 7 Molten fraction and crystallization rate versus temperature on reheating for neat PBAT and PBAT/organoclay nanocomposites with C10A (**a**, **b**), C20A (**c**, **d**) and C30B (**e**, **f**)

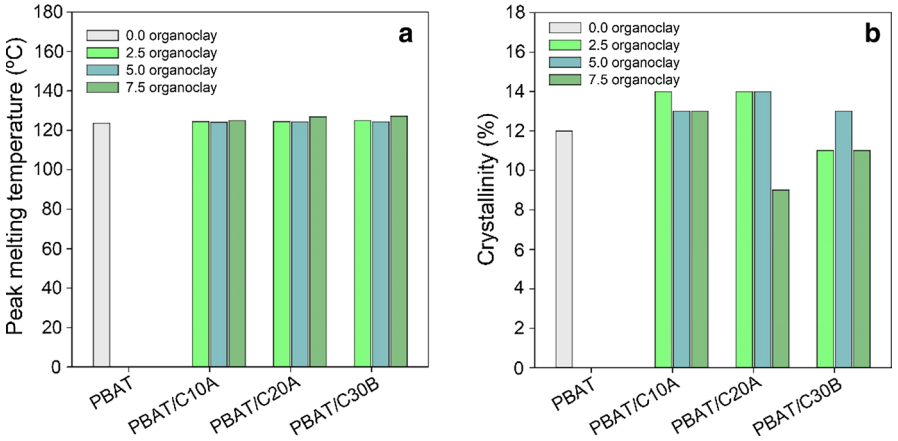

Fig. 8 Peak melting temperature (**a**) and crystallinity (**b**) for PBAT and nanocomposites

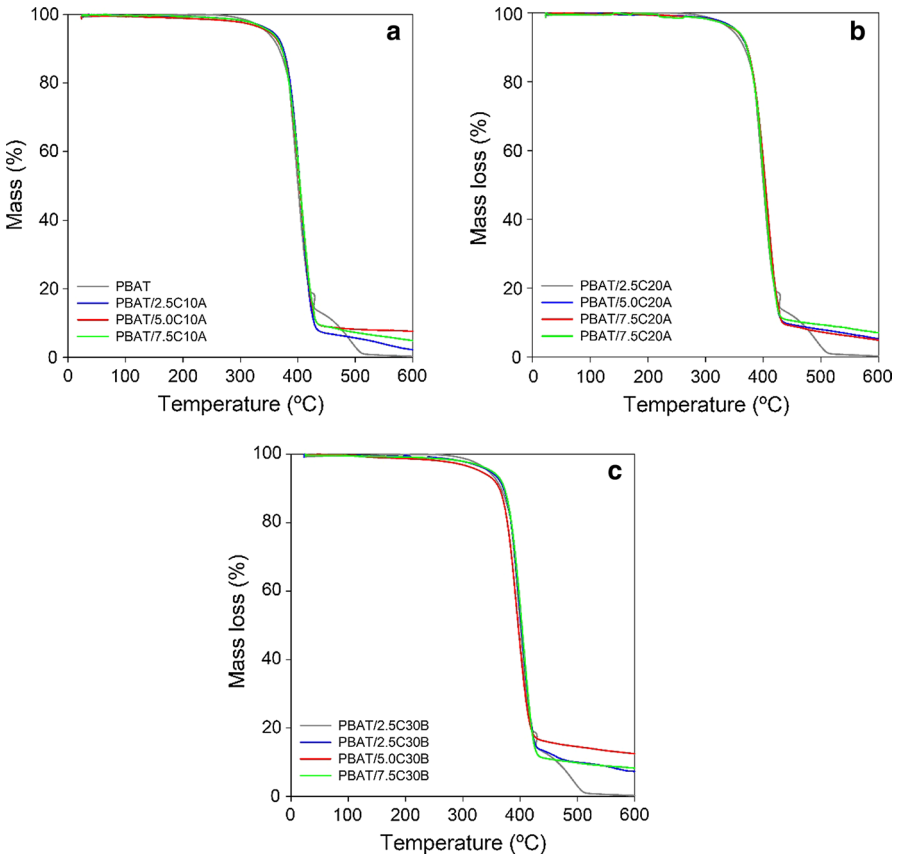

Fig. 9 TG curves PBAT/organoclay nanocomposites with C10A (**a**), C20A (**b**) and C30B (**c**)

Dynamic mechanical analysis

Figure 10 shows the storage modulus (E′) versus temperature for neat PBAT and for the nanocomposites investigated.

As expected, nanocomposite's storage modulus (E′) increases with organoclay content as the modulus of these fillers are higher than that of the matrix. In all systems, organoclay incorporation led to increases in elastic modulus with clay concentration (2× to 3×) and is virtually independent of organoclay identity. The modulus of the systems, which ranged from 2.5 to 4 GPA at − 60 °C decreased with increasing temperatures to 0.1 GPa at 80 °C. Similar results are reported in other PBAT/organoclay compound systems [17].

Figure 11 shows damping factor (tan δ) curves of PBAT and PBAT/organoclays.

The observed glass transition peak for PBAT was around − 28.5 °C, as reported in the literature [17, 18]. Our data indicates *Tg* of the nanocomposites to be slightly

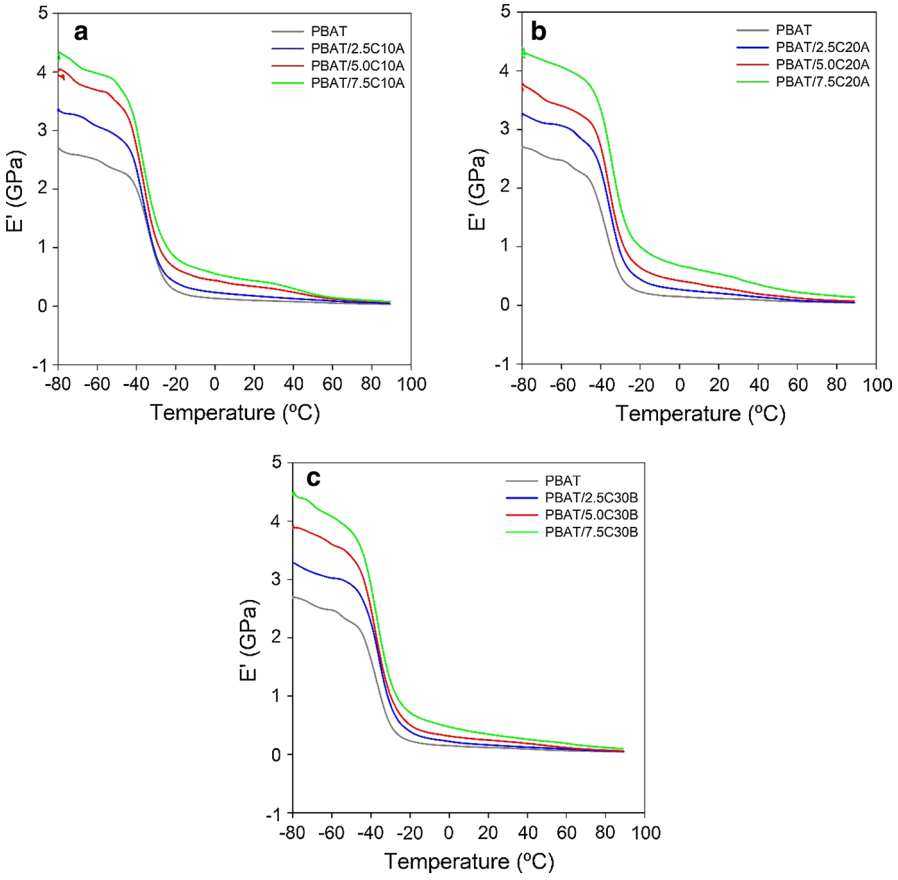

Fig. 10 Storage modulus for neat PBAT and PBAT/organoclay nanocomposites with C10A (**a**), C20A (**b**) and C30B (**c**)

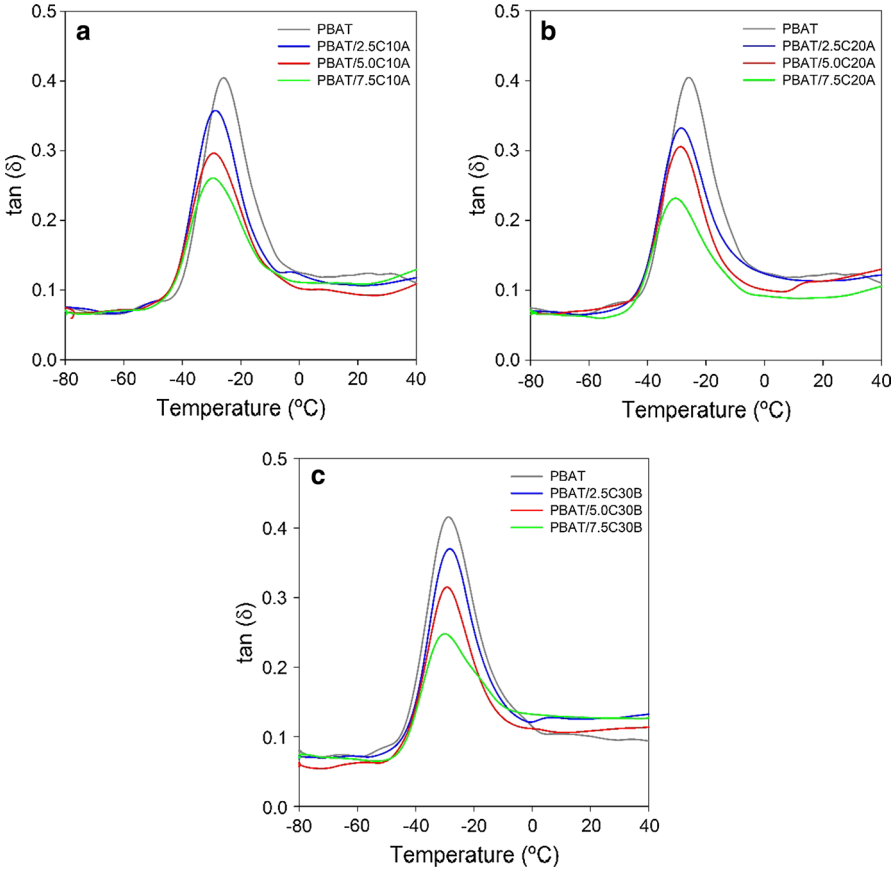

Fig. 11 Damping factor for neat PBAT and PBAT/organoclay nanocomposites with C10A (**a**), C20A (**b**) and C30B (**c**)

Table 4 Glass transition temperature (in °C) of the nanocomposites

Clay content (%)	PBAT/C10A	PBAT/C20A	PBAT/C30B
0.0	− 25.8	− 25.8	− 28.6
2.5	− 28.6	− 28.5	− 28.3
5.0	− 28.9	− 28.5	− 29.2
7.5	− 29.6	− 30.4	− 30.2

lower than that of PBAT and essentially independent of clay identity as shown in Table 4.

Conclusions

Incorporation of organoclays lead to nanocomposites of significantly intercalated structures, with interlayer spacing virtually independent of clay identity and concentration. No substantial exfoliation was observed. XRD results were consistent with TEM images. A substantial decrease in crystallization temperature, particularly in nanocomposites prepared with Cloisite 30B, without significant changes in the degree of crystallinity was obtained. These results are attributed to the nucleating effect of the clay nanoparticles. Organoclay incorporation leads to nanocomposites with slightly higher thermal stability than that of the neat polymer. The elastic modulus depends on clay concentration but is independent of the organoclay identity. The glass transition temperature is insensitive to clay content and identity.

In general, similar behavior was displayed by composites prepared with the three organoclays (C10A, C20A and C30B) employed in this work. However, the slightly more polar organoclay (C30B) had a larger effect on PBAT melt crystallization temperature.

Acknowledgements The authors grateful to the Conselho Nacional de Pesquisa (CNPQ-Brazil), Grant #463622/2013-0, to the Coordenação de Aperfeiçoamento do Ensino Superior (CAPES-Brazil) and to the Erasmus Mundus Program for financial support.

References

1. Avérous L, Pollet E (2012) Environmental silicate nano-biocomposites. Springer, London
2. Ray SS, Bousmina M (2005) Biodegradable polymers and their layered silicate nanocomposites. In: Greening the 21st century materials world. Progress in Materials Science, pp 962–1079
3. Bordes P, Hablot E, Pollet E, Avérous L (2009) Effect of clay organomodifiers on degradation of polyhydroxyalkanoates. Polym Deg Stab 94:789–796
4. Falcão GAM, Almeida TG, Bardi MAG, Carvalho LH, Canedo EL (2018) PBAT/organoclay composite films—part 2: effect of UV aging on permeability, mechanical properties and biodegradation. Polym Bull. https://doi.org/10.1007/s00289-018-2385-z
5. Yamamoto M, Witt U, Skupin G, Beimborn D, Müller RJ (2002) Biodegradable aliphatic-aromatic polyesters: Ecoflex. In: Steinbüchel YDA (ed) Biopolymers—polyesters III—applications and commercial products. Wiley, New York, p 299
6. Chen JH, Chen CC, Yang MC (2011) Characterization of nanocomposites of poly (butylene adipate-co-terephthalate) blending with organoclay. J Polym Res 18:2151–2159
7. Fukushima K, Rasyida A, Yang MC (2013) Biocompatibility of organically modified nanocomposites based on PBAT. J Polym Res 20:302
8. Falcão GAM, Vitorino MBC, Almeida TG, Bardi MAG, Carvalho LH, Canedo EL (2017) PBAT/organoclay composite films: preparation and properties. Polym Bull 74:4423–4436
9. Someya Y, Sugahara Y, Shibata M (2005) Nanocomposites based on poly(butylene adipate-co-terephthalate) and montmorillonite. J App Polym Sci 95:386–392
10. Mondal D, Bhowmick B, Maity D, Mollick MMR, Rana D, Rangarajan V, Sen R, Chattopadhyay D (2015) Investigation on sodium benzoate release from poly(butylene adipate-co-terephthalate)/organoclay/sodium benzoate based nanocomposite film and their antimicrobial activity. J Food Sci 80:602–609

11. Strawhecker K, Manias E (2000) Structure and properties of poly(vinyl alcohol)/Na + montmorillonite nanocomposites. Chem Mater 12:2943–2949
12. Alexandre M, Dubois P (2000) Polymer-layered silicate nanocomposites: preparation, properties and uses of a new class of materials. Mater Sci Eng 28:1–63
13. Bouakaz BS, Habi A, Grohens Y, Pillin I (2018) Effect of combinations of nanofillers on rheology-structure relations in biodegradable poly(ε-caprolactone) nanocomposites. Appl Clay Sci 161:35–47
14. Olivares-Maldonado Y, Ramırez-Vargas E, Sánchez-Valdés S, Ramos-DeValle LF, Rodriguez-Fernandez OS, Espinoza-Martınez AB, Medellın-Rodrıguez FJ, Lozano-Ramirez T (2014) Effect of organoclay structure characteristics on properties of ternary PP-EP/EVA/nanoclay blend systems. Polym Compos 35:2241–2250
15. Someya Y, Kondo N, Shibata M (2007) Biodegradation of poly(butylene adipate-co-butylene terephthalate)/layered-silicate nanocomposites. J Appl Polym Sci 106:730–736
16. Yang F, Qiu Z (2011) Preparation, crystallization, and properties of biodegradable poly(butylene adipate-co-terephthalate)/organomodified montmorillonite nanocomposites. J Appl Polym Sci 119:1426–1434
17. Mohanty S, Nayak SK (2010) Biodegradable nanocomposites of poly (butylene adipate-co-terephthalate) (PBAT) with organically modified nanoclays. Int J Plast Technol 14:192–212
18. Chen J-H, Yang M-C (2015) Preparation and characterization of nanocomposite of maleated poly(butylene adipate-co-terephthalate) with organoclay. Mater Sci Eng, C 46:301–308
19. BYK Additives (2018) Cloisite® 10A Nanoclay—Technical Data Sheet. BYK Additives, Cloisite® 20A Nanoclay—Technical Data Sheet. BYK Additives, Cloisite® 30B Nanoclay—Technical Data Sheet
20. Canedo EL, Wellen RMR, Almeida YMB (2016) Cristalização de Polímeros: Tratamento de Dados e Modelagem Macrocinética. ANP—PRH28/UFPE, Recife
21. Wellen RMR, Canedo EL (2015) Complex cold crystallization peaks in PET/PS blends. Polym Test 41:26–32
22. Ries A, Canedo EL, Wellen RMR (2016) Non-isothermal cold crystallization kinetics of poly(3-hydoxybutyrate) filled with zinc oxide. Thermochim Acta 637:74–81
23. Vitorino MBC, Cipriano PB, Wellen RMR, Canedo EL, Carvalho LH (2016) Nonisothermal crystallization of poly(β-hydroxybutyrate)/babassu eco-composites. Kinetics of crystallization. J Thermal Anal Calorim 126:755–769
24. Jaques NG, Silva IDS, Ries A, Canedo EL, Wellen RMR (2018) Nonisothermal crystallization studies of PBT/ZnO compounds. Ozawa and Mo models. J Thermal Anal Calorim 131:2569–2577
25. Sousa FM, Costa ARM, Reul LTA, Cavalcanti FB, Carvalho LH, Almeida TG, Canedo EL (2018) Rheological and thermal characterization of PCL/PBAT blends. Polym Bull. https://doi.org/10.1007/s00289-018-2428-5
26. Herrera R, Franco L, Rodriguez-Galán A, Puiggalí J (2002) Characterization and degradation behavior of poly(butylene adipate-co-terephthalate)s. J Polym Sci A: Polym Chem 40:4141–4157
27. Almeida TG, Costa ARM, Wellen RMR, Canedo EL, Carvalho LH (2017) PHB/bentonite compounds. Effect of clay modification and thermal aging on properties. Mater Res 20:1503–1510
28. Utracki LA (2004) Clay-containing polymeric nanocomposites. Rapra Technology, Shawbury
29. Bhattacharya SN, Gupta RK, Kamal MR (2008) Polymeric nano-composites. Hanser, Munich
30. Wypych George (2016) Handbook of nucleating agents. ChemTec Publishing, Toronto
31. Chieng BW, Ibrahim NA, Wan Yunus WMZ (2010) Effect of organo-modified montmorillonite on poly(butylene succinate)/poly(butylene adipate-co-terephthalate) nanocomposites. Express Polym Lett 4:404–414
32. Agag T, Koga T, Takeichi T (2001) Studies on thermal and mechanical properties of polyimide-clay nanocomposites. Polym 42:3399–3408